Appendix: Distinguishability and many-particle interference

Adrian J. Menssen[1,*], Alex E. Jones[1,2,*], Benjamin J. Metcalf[1],
Malte C. Tichy[3], Stefanie Barz[1], W. Steven Kolthammer[1], Ian A. Walmsley[1]
[1] *Clarendon Laboratory, Department of Physics, University of Oxford, OX1 3PU, United Kingdom,*
[2] *Blackett Laboratory, Imperial College London, SW7 2BW, United Kingdom,*
[3] *Department of Physics and Astronomy, University of Aarhus, DK-8000 Aarhus C, Denmark*
[*] *These authors contributed equally to this work.*

ADDITIONAL THEORY

Transition probability for three partially distinguishable bosons in a three mode-setup

We inject three partially distinguishable bosons into the three input modes of a scattering setup described by a unitary matrix U. The distinguishing degrees of freedom of the bosons – in our case the photon polarisation and the time-of-arrival – are described by the states $|\phi_1\rangle, |\phi_2\rangle, |\phi_3\rangle$. The mutual pairwise distinguishabilities are then encoded in the positive semi-definite hermitian matrix $\mathcal{S}_{j,k} = \langle\phi_j|\phi_k\rangle = r_{jk}e^{i\varphi_{jk}}$, which accommodates both the scalar product moduli r_{jk} as well as the relative phases φ_{jk}. The probability to find one particle in each output mode is obtained as a sum over all possible double-sided Feynman diagrams [1], giving a multidimensional permanent

$$P_{111} = \sum_{\sigma,\rho\in S_3}\prod_{j=1}^{3} U_{\sigma_j,j}U^{\star}_{\rho_j,j}\mathcal{S}_{\rho_j,\sigma_j}, \tag{1}$$

comprising fully distinguishable particles ($\mathcal{S} = \mathrm{diag}(1,1,1)$, $r_{jk} = \delta_{j,k}$) and perfectly identical bosons ($\mathcal{S}_{j,k} = 1$, $r_{jk} = 1$) as extremal cases.

Our aim is to understand the dependence of three-photon interference on the distinguishability parameters r_{jk} and φ_{jk} in detail. For this purpose, we write out the sums over the permutation group S_3 explicitly,

$$\begin{aligned} P_{111} = {} & \mathrm{perm}(U * U^{\star}) + r_{12}^2\,\mathrm{perm}(U * U^{\star}_{2,1,3}) + r_{31}^2\,\mathrm{perm}(U * U^{\star}_{3,2,1}) + r_{23}^2\,\mathrm{perm}(U * U^{\star}_{1,3,2}) \\ & + 2\Re\{r_{12}r_{23}r_{31}e^{i(\varphi_{12}+\varphi_{23}+\varphi_{31})}\mathrm{perm}(U * U^{\star}_{2,3,1})\}, \end{aligned} \tag{2}$$

where $U^{\star}_{x,y,z}$ is the element-wise complex conjugated matrix $U^{\star}$ with the *rows* (corresponding to the input modes) permuted as $(1,2,3) \to (x,y,z)$, i.e. for $(x,y,z) = (1,2,3)$, we leave the matrix unchanged, while for $(x,y,z) = (2,1,3)$, we exchange the first two rows. The product $X * Y$ is meant as Hadamard element-wise multiplication, not the usual matrix-product.

For final states with s_j particles in the jth output mode, we adapt Eqn. (2) formally by replacing U by a matrix of the same dimensions that repeats the jth column of U s_j times , i.e. the column multiplicity reflects the final mode population. To ensure the proper normalization of the final result, a factor $(\prod_{j=1}^{3} s_j!)^{-1}$ needs to be included, where $\boldsymbol{s} = (s_1, s_2, s_3)$ is the mode occupation list of the final state.

We see clearly how the dependence on the scattering matrix U is separated from the dependence on the scalar products $\mathcal{S}$. For a fixed scattering matrix U, the output signals depend on precisely six parameters, $r_{12}, r_{31}, r_{23}, \varphi_{12}, \varphi_{23}, \varphi_{31}$, of which only four have physical significance: the three scalar product moduli r_{12}, r_{23}, r_{31} and the collective triad phase $\varphi = \varphi_{12} + \varphi_{23} + \varphi_{31}$. Whereas each relative phase φ_{jk} can be transformed away by a global phase transformation, the *sum* of the three relative phases – the collective triad phase φ – remains independent of any choice of basis or global phase. The dependence of scattering probabilities on a phase that describes the particles' collective indistinguishability has no precedent in single- or two-particle scattering. The triad phase only carries physical meaning in the context of the full three-particle state, and is thus a purely collective quantity.

Event probabilities in the symmetric tritter

For a symmetric tritter,

$$U = \frac{1}{\sqrt{3}} \begin{pmatrix} 1 & 1 & 1 \\ 1 & e^{i\frac{4\pi}{3}} & e^{i\frac{2\pi}{3}} \\ 1 & e^{i\frac{2\pi}{3}} & e^{i\frac{4\pi}{3}} \end{pmatrix}, \tag{3}$$

the output event probabilities take particularly simple forms:

$$P_{111} = \frac{1}{9}\left[2 + 4\, r_{12}r_{23}r_{31}\cos(\varphi) - r_{12}^2 - r_{23}^2 - r_{31}^2\right] \tag{4}$$

$$P_{300} = P_{030} = P_{003} = \frac{1}{27}\left(1 + r_{12}^2 + r_{23}^2 + r_{31}^2 + 2r_{12}r_{23}r_{31}\cos(\varphi)\right), \tag{5}$$

$$P_{120} = P_{012} = P_{201} = \frac{1}{9}\left(1 - 2r_{12}r_{23}r_{31}\cos(\varphi + \pi/3)\right), \tag{6}$$

$$P_{021} = P_{210} = P_{102} = \frac{1}{9}\left(1 - 2r_{12}r_{23}r_{31}\cos(\varphi - \pi/3)\right). \tag{7}$$

Here, P_{ijk} denotes the probability of measuring i photons in output mode 1, j photons in output mode 2, and k photons in output mode 3. The probability to find two particles in one output mode vanishes for indistinguishable photons, a result of the suppression law for Fourier matrices [2].

INTERNAL SPACE DIMENSIONALITY AND TRIAD PHASE

The triad phase $\varphi = \varphi_{12} + \varphi_{23} + \varphi_{31}$ encodes a purely collective property, which can only take non-trivial values for partially distinguishable particles: If all pairs of particles are mutually perfectly indistinguishable, we have $r_{ij} = 1$, such that $|\phi_1\rangle \propto |\phi_2\rangle \propto |\phi_3\rangle$. The three states then span a trivial one-dimensional Hilbert-space, and $\varphi = 0$. On the other hand, when the particles are fully distinguishable, all scalar products r_{12}, r_{23}, r_{31} vanish, and the value of the phase φ is neither defined, nor does it have any impact on any observable, since it comes only in conjunction with the product $r_{12}r_{23}r_{31}$. In this case, the three states span a three-dimensional Hilbert-space.

In the intermediate case in which all particles are neither mutually distinguishable nor indistinguishable ($0 < r_{ij} < 1$ for all $i \neq j$), the question arises whether the three internal states $|\phi_1\rangle, |\phi_2\rangle, |\phi_3\rangle$ span a three- or merely a two-dimensional Hilbert-space. This question arises, e.g. when three photons are deliberately prepared in different polarisation states, but are supposed to be indistinguishable in all other degrees of freedom.

In order to see how the measurement of the triad phase φ can resolve this question, let us first consider three states living in a qubit-like two-dimensional Hilbert-space. Without restrictions to generality, we can then find two states $|0\rangle$ and $|1\rangle$, such that

$$|\phi_1\rangle = |0\rangle \tag{8}$$

$$|\phi_2\rangle = \cos\alpha|0\rangle + \sin\alpha|1\rangle \tag{9}$$

$$|\phi_3\rangle = \cos\beta|0\rangle + e^{i\gamma}\sin\beta|1\rangle, \tag{10}$$

where $0 < \alpha, \beta < \pi/2$, $0 \leq \gamma < 2\pi$. We note that the three states are described by three parameters – precisely those required to describe the relative positions of three points on a Bloch-sphere describing a qubit. In Eqn. 4 (main paper), however, four parameters – $r_{12}, r_{23}, r_{31}, \varphi$ – dictate the degree of three-particle interference.

By evaluating the relevant scalar products

$$\langle\phi_1|\phi_2\rangle = \cos\alpha \tag{11}$$

$$\langle\phi_2|\phi_3\rangle = \cos\alpha\cos\beta + e^{-i\gamma}\sin\alpha\sin\beta \tag{12}$$

$$\langle\phi_3|\phi_1\rangle = \cos\beta, \tag{13}$$

we can express γ as a function of r_{12}, r_{23}, r_{31}, to see that φ is fixed by the three scalar product moduli r_{12}, r_{23}, r_{31}, i.e.

$$\varphi = \varphi_{2d}(r_{12}, r_{23}, r_{31}) \tag{14}$$

In that sense, when restricted to a qubit-like Hilbert-space, the triad phase is not an independent degree of freedom, but it is fully fixed by the geometry of the three vectors on the Bloch sphere, or, equivalently, by r_{12}, r_{23}, r_{31}.

When we lift the restriction to a qubit-like Hilbert-space and admit states of the more general form

$$|\phi_1\rangle = |0\rangle \tag{15}$$
$$|\phi_2\rangle = \cos\alpha|0\rangle + \sin\alpha|1\rangle \tag{16}$$
$$|\phi_3\rangle = \cos\epsilon\cos\beta|0\rangle + \cos\epsilon e^{i\gamma}\sin\beta|1\rangle + \sin\epsilon|2\rangle, \tag{17}$$

the new parameter ϵ describes to what extent the third state $|\phi_3\rangle$ lives outside the Hilbert-space spanned by $|\phi_1\rangle$ and $|\phi_2\rangle$. Hence, we now need four parameters to describe the three states, and even when r_{12}, r_{23}, r_{31} are fixed, φ now remains an independently tuneable parameter.

As a consequence, the three-photon measurements yielding r_{12}, r_{23}, r_{31} and φ reveal whether or not the three states $|\phi_1\rangle, |\phi_2\rangle, |\phi_3\rangle$ span a three-dimensional Hilbert-space ($\epsilon > 0$) or merely a two-dimensional one ($\epsilon = 0$). The latter is clearly a collective property of all three states, and invisible to any combination of two-photon measurement data, which only yield r_{12}, r_{23}, r_{31}, but not the triad phase φ. In an experiment, a measurement of φ that is compatible to $\varphi_{2d}(r_{12}, r_{23}, r_{31})$ implies that the three photons live in a two-dimensional space, while a measurement φ that is incompatible with $\varphi_{2d}(r_{12}, r_{23}, r_{31})$ shows that the three photons are distinguishable in more than a qubit-like degree of freedom.

DEPENDENCE OF TRIAD PHASE ON DELAY IN THREE-PHOTON INTERFERENCE

A single photon in spectral mode Ψ is denoted

$$|\Psi\rangle = \int \mathrm{d}\omega\tilde{\psi}(\omega)|\omega\rangle \tag{18}$$

where the state of a single photon with angular frequency ω is given by $|\omega\rangle$ and the mode is described by the complex-valued spectral amplitude $\tilde{\psi}(\omega)$. The same state can be described in the temporal domain with the mode transformation $|\omega\rangle = (2\pi)^{-1/2}\int \mathrm{d}\tau \exp(i\omega\tau)|\tau\rangle$, where $|\tau\rangle$ describes a single photon with arrival time τ. With this substitution, we find $|\Psi\rangle = \int \mathrm{d}\tau\psi(\tau)|\tau\rangle$ where the temporal amplitude $\psi(\tau)$ is the inverse Fourier transform of $\tilde{\psi}(\omega)$.

If we delay a single photon initially in mode Ψ by a time t, the resulting state is

$$|t\rangle_\psi \equiv \int \mathrm{d}\tau\psi(\tau - t)|\tau\rangle = \int \mathrm{d}\omega e^{-it\omega}\tilde{\psi}(\omega)|\omega\rangle. \tag{19}$$

In the following, we write this as $|t\rangle$ and forgo the subscript since only one initial mode will be considered. The inner product of two single-photons in initial mode Ψ delayed by times t_1 and t_2 is

$$\langle t_1|t_2\rangle = \int \mathrm{d}\omega e^{-i(t_2-t_1)\omega}|\tilde{\psi}(\omega)|^2 = \mathcal{F}\left[|\tilde{\psi}|^2\right](t_2 - t_1) \equiv \zeta(t_{21}) \tag{20}$$

where the function ζ is defined as the Fourier transform of the spectral intensity $|\tilde{\psi}(\omega)|^2$ and $t_{ij} = t_i - t_j$.

Now consider the triad phase of three photons each in initial mode Ψ with a distinct delay

$$\varphi = \arg\left[\langle t_1|t_2\rangle\langle t_2|t_3\rangle\langle t_3|t_1\rangle\right] = \arg\left[\langle t_1|t_2\rangle\right] + \arg\left[\langle t_2|t_3\rangle\right] + \arg\left[\langle t_3|t_1\rangle\right]. \tag{21}$$

We are interested in the conditions for which φ is independent of the delays. Accordingly we require that derivative with respect to delay vanishes

$$\begin{aligned}\frac{\mathrm{d}\varphi}{\mathrm{d}t_1} &= \frac{\partial\varphi}{\partial(t_{21})}\frac{\mathrm{d}(t_{21})}{\mathrm{d}t_1} + \frac{\partial\varphi}{\partial(t_{13})}\frac{\mathrm{d}(t_{13})}{\mathrm{d}t_1} \\ &= \frac{\mathrm{d}}{\mathrm{d}s}\big[\arg\zeta(s)\big]\Big|_{t_{13}} - \frac{\mathrm{d}}{\mathrm{d}s}\big[\arg\zeta(s)\big]\Big|_{t_{21}} = 0.\end{aligned} \tag{22}$$

For this to be true for all values of t_2 and t_3, it must be that $\frac{\mathrm{d}}{\mathrm{d}s}\left[\arg\zeta(s)\right]$ is independent of s. Therefore $\arg\zeta(s)$ is linear

$$\arg\zeta(s) = \theta_0 + \Omega s. \tag{23}$$

The inverse Fourier transform of ζ, the spectral intensity, is real. It follows that $\zeta(-s) = \zeta(s)^*$. Therefore, $\arg\zeta(s)$ is odd and $\theta_0 = 0$.

If φ is independent of the delays, we can therefore write

$$\zeta(s) = |\zeta(s)|e^{i\Omega s} = \mathcal{F}\left[|\tilde{\psi}(\omega)|^2\right](s). \tag{24}$$

Consider spectral intensity functions for which $\Omega = 0$, which we denote as $|\tilde{\psi}_0(\omega)|^2$. For this case, since $|\tilde{\psi}_0(\omega)|^2$ and its Fourier transform ζ are real valued, $|\tilde{\psi}_0(\omega)|^2$ is an even function. Now consider the general case $|\tilde{\psi}_\Omega(\omega)|^2$ for non-zero Ω. The shift property of the Fourier transform along with Eqn. (24) tells us that $|\tilde{\psi}_\Omega(\omega - \Omega)|^2$ is an even function. Therefore we conclude that the triad phase φ is independent of delays if the three photons start in identical spectral modes for which the spectral intensity is symmetric about its mean value.

INNER PRODUCTS OF GAUSSIAN WAVEPACKETS WITH RELATIVE DELAYS

The state of a single photon in the time-frequency modes (τ, ω), delayed by time t is given by:

$$|t\rangle = \int d\tau \phi(\tau - t)|\tau\rangle \tag{25}$$

For a Gaussian wave-packet delayed by time t, central frequency Ω and variance in time σ^2, $\phi(\tau; t)$ takes the form:

$$\phi(\tau - t) = \left(\frac{1}{\pi\sigma^2}\right)^{1/4} e^{-\frac{(\tau-t)^2}{2\sigma^2} + i\Omega(t-\tau)} \tag{26}$$

We can express the overlap of the temporal modes of two photons with identical Gaussian spectra at times t_1 and t_2 as:

$$\langle t_1|t_2\rangle = \int_{-\infty}^{\infty} \phi^*(\tau - t_1)\phi(\tau - t_2)d\tau = e^{-\frac{(t_1-t_2)^2}{4\sigma^2} - i\Omega(t_1-t_2)} \tag{27}$$

Next, we show that for time-delays the products of overlaps that appear in the expressions for the multi-photon coincidence probabilities are always real and positive and hence do not give rise to a triad phase. In the case of the two photon interference terms, which contain expressions of the form

$$\langle t_1|t_2\rangle\langle t_2|t_1\rangle = |\langle t_1|t_2\rangle|^2 \tag{28}$$

this is easy to see, as the expression is purely real. For the three photon interference term:

$$\langle t_1|t_2\rangle\langle t_2|t_3\rangle\langle t_3|t_1\rangle = e^{-((t_1-t_2)^2+(t_2-t_3)^2+(t_3-t_1)^2)/(4\sigma^2) - i\Omega(t_1-t_2+t_2-t_3+t_3-t_1)} = e^{-((t_1-t_2)^2+(t_2-t_3)^2+(t_3-t_1)^2)/(4\sigma^2)} \tag{29}$$

As we can see this expression is also real. This also holds for any number of photons.

EXPERIMENTAL DETAILS

We pump three separate waveguides in a silica-on-silicon chip [3] with a Ti-Saph femtosecond pulsed laser running at 80 MHz and 740 nm (130 fs pulses). In each guide, we generate one signal and one idler photon at 680 nm and 817 nm, respectively. The pump has an orthogonal polarisation to the daughter photons and so can be separated using a polarising beam splitter after the chip. The signal and idler are spatially separated using a dichroic mirror before final filtering to remove residual pump and to factor out their spectral components, removing spectral correlations to give pure single photons. Pumping three of these guides yields three signal photons and three idler photons. By heralding on the former using three silicon APDs, we are left with three heralded, highly pure identical single photons with central wavelength 817 nm at a rate of about 0.5 Hz when pumping with 130 mW per guide. The setup for measuring different output configurations after the interference tritter is shown in Fig. 1.

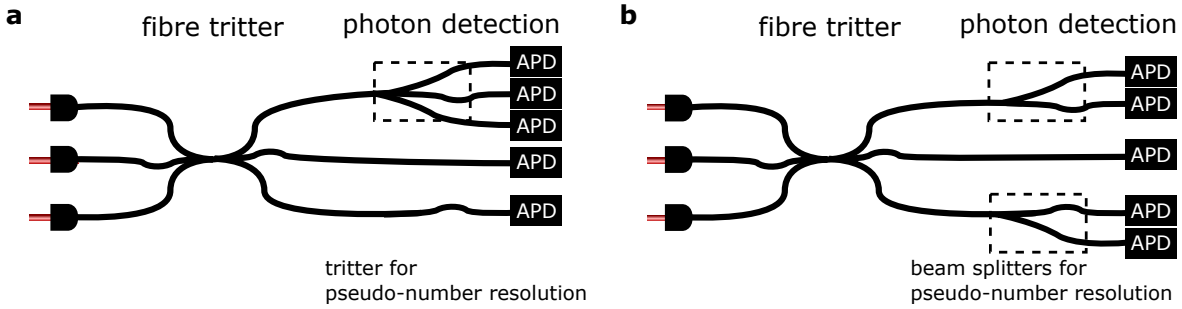

Figure 1. In our experiment we use additional fibre beam splitters and tritters to allow pseudo-number resolution. **a.** For monitoring genuine three-photon interference, the first and third outputs are connected to fibre beam splitters. **b.** For probing the triad phase, we used a single tritter on the first output mode of the interference tritter.

RAW EXPERIMENTAL DATA

Polarisations set for $\varphi = 0$ (cf. Equation 7 in main paper)

HOM dips for temporal alignment of photons

In order to align the generated photons temporally and verify their indistinguishability, we perform heralded HOM measurements for the three possible pairs injected into the tritter. We also use these to verify our polarisation state preparations. The results are shown in the Figures below.

For the case where the photons have identical polarisation, we expect a theoretical visibility of 50% (since the two-photon coincidence probability is $P_{110} = \frac{1}{9} \times (2 - |\langle\phi_1|\phi_2\rangle|^2)$ for a tritter, and so the visibility should be half the squared scalar product magnitude), we record closer to 40% due to all effects mentioned in the main paper. The dip in Figure 2 is twice as narrow as the others, corresponding to the dip between two photons that are both being translated in time on injection. The other two dips are from when only one of the photons injected into the tritter is translated in time (see Figure 3 in main text). The dips are all centred such that the three photons overlap in time when the stages are at their zero positions.

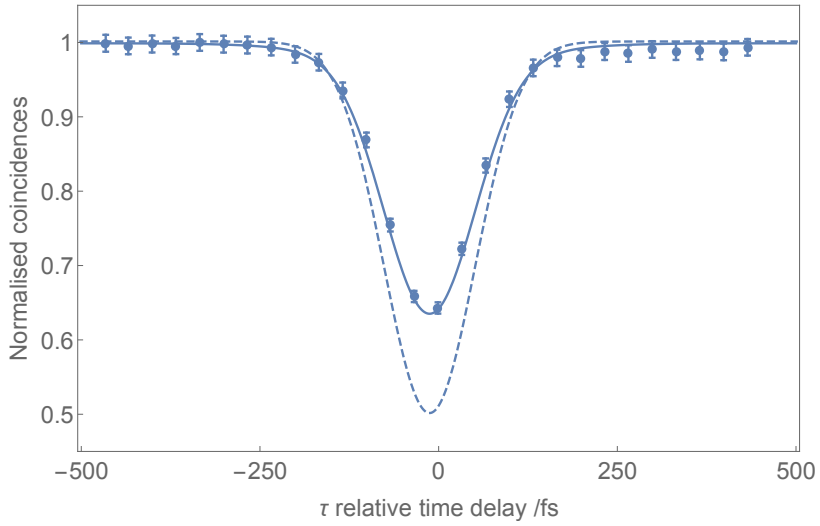

Figure 2. Plot of normalised heralded two-photon coincidences through the tritter when the injected photons have identical polarisations. In this case we inject photons into the first and second tritter inputs and monitor the first and second output ports. The solid line is the model curve, whilst the dashed line is an ideal theory curve. The model yields a visibility of 36%, while for the ideal curve the visibility is 50%. The FWHM of the model dip is $\sim$ 150 fs.

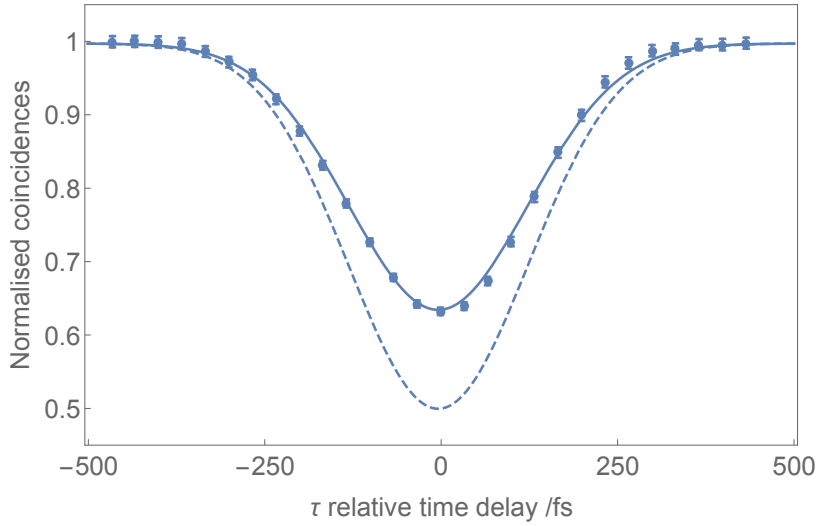

Figure 3. Plot of normalised heralded two-photon coincidences through the tritter when the injected photons have identical polarisations. In this case we inject photons into the first and third tritter inputs and monitor the first and third output ports. The solid line is the model curve, whilst the dashed line is an ideal theory curve. The model yields a visibility of 36%, while for the ideal curve the visibility is 50%. The FWHM of the model dip is $\sim$ 300 fs.

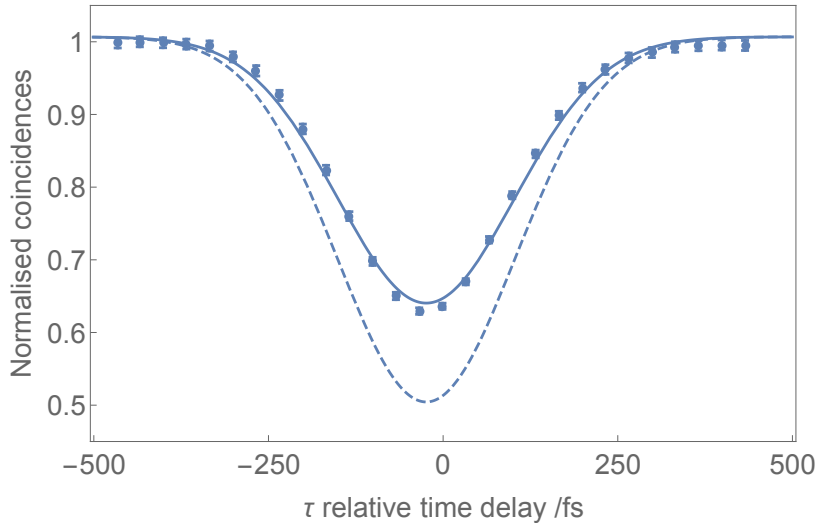

Figure 4. Plot of normalised heralded two-photon coincidences through the tritter when the injected photons have identical polarisations. In this case we inject photons into the second and third tritter inputs and monitor the second and third output ports. The solid line is the model curve, whilst the dashed line is an ideal theory curve. The model yields a visibility of 36%, while for the ideal curve the visibility is 50%. The FWHM of the model dip is $\sim$ 300 fs.

Additional output event plots

Here we present plots for count rates corresponding to $P_{210}, P_{201}, P_{300}$ in the case where all photons are injected into the tritter with the same polarisation. In the ideal case when all photons are completely indistinguishable in time and polarisation, $P_{210} = P_{201} = 0$ and these outputs are completely suppressed [2]. Our simulations demonstrate this is not the case when taking into account experimental imperfections, and the visibility is reduced from 100% to around 57%. The theory and simulation curves have been rescaled for comparison with experimental count rates.

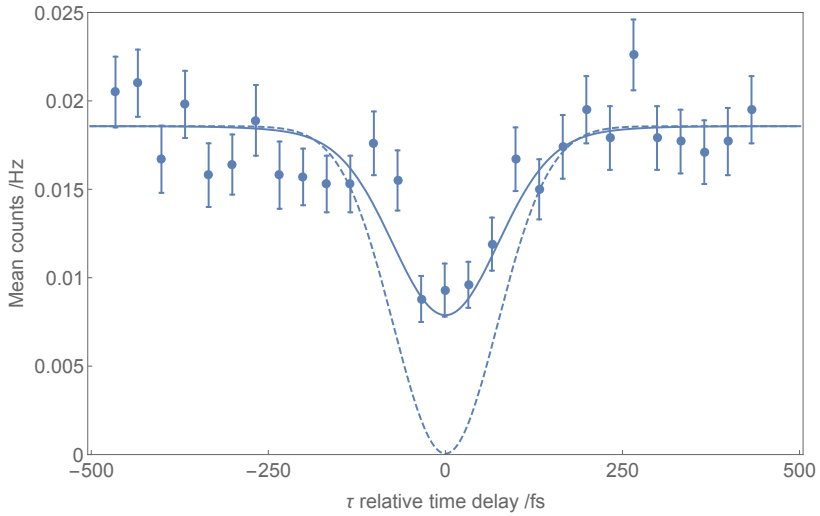

Figure 5. Plot of mean counts for the outputs corresponding to P_{210} as illustrated in Figure 1a. The model yields a visibility of 57%, while for the ideal curve the visibility is 100%. The FWHM of the model dip is $\sim$ 180 fs.

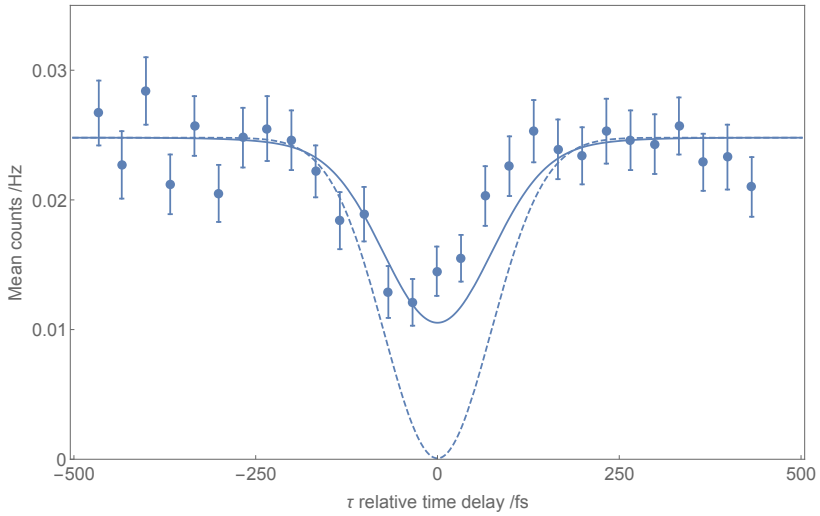

Figure 6. Plot of mean counts for the outputs corresponding to P_{201} as illustrated in Figure 1a. The solid line is the model curve, whilst the dashed line is an ideal theory curve. The model yields a visibility of 57%, while for the ideal curve the visibility is 100%. The FWHM of the model dip is $\sim$ 180 fs.

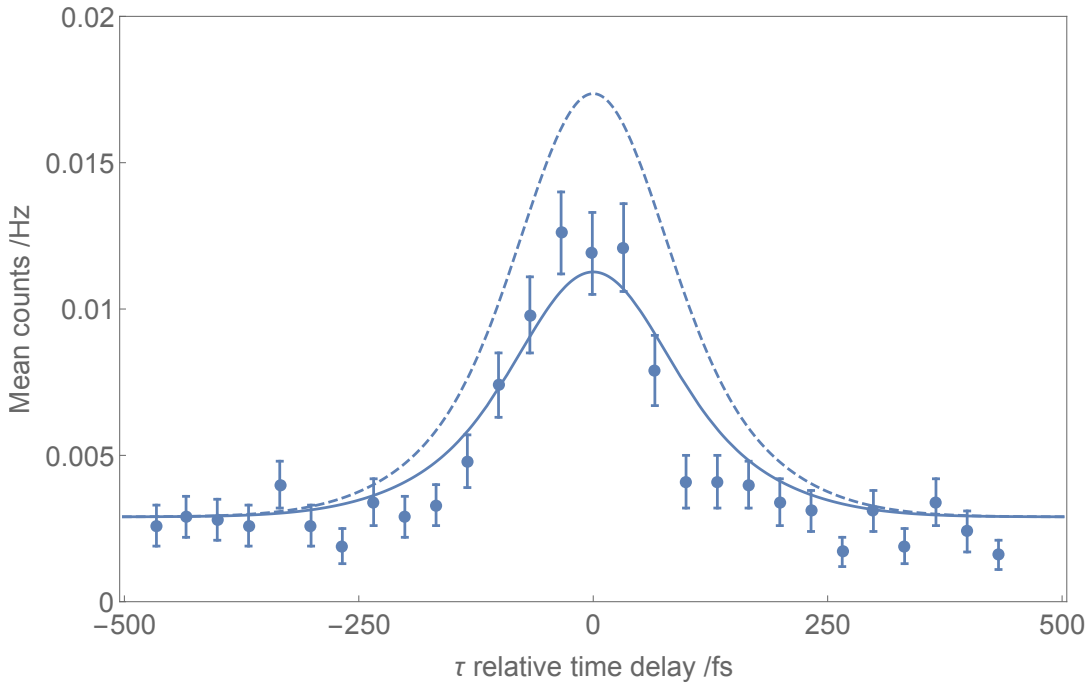

Figure 7. Plot of count rates corresponding to P_{300} as measured using the setup in Figure 1a, when all photons have the same polarisation.

Polarisations set for $\varphi = \pi$ (cf. Equation 8 in main paper)

HOM dips for temporal alignment of photons

Again to align the three photons temporally before injection into the tritter, we perform HOM measurements for the three pairs of photons. We expect 12.5% visibility but record closer to 10%, again due to the effects mentioned in the main paper. The dip in Figure 8 is twice as narrow as the others, corresponding to the dip between two photons which are both being translated in time on injection. The other two dips are from when only one of the photons injected into the tritter is translated in time (see Figure 3 in main text). The dips are all centred such that the three photons overlap in time when the stages are at their zero positions.

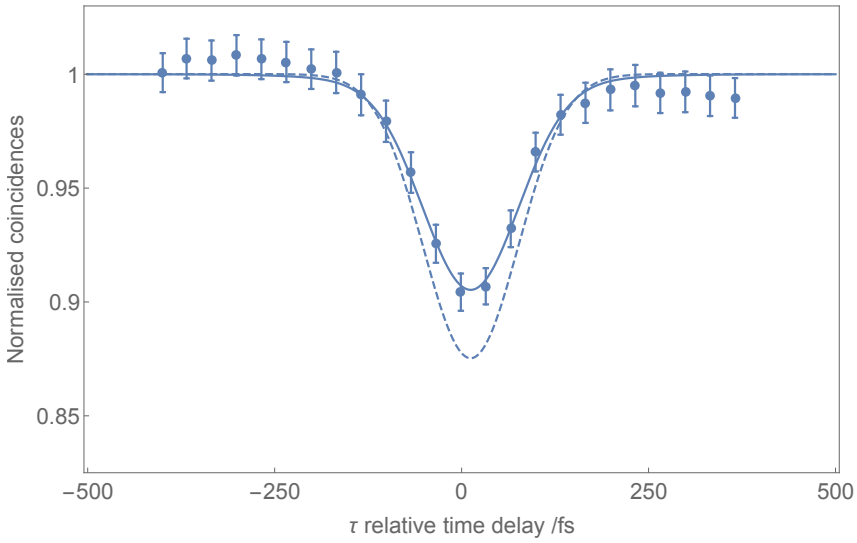

Figure 8. Plot of normalised heralded two-photon coincidences through the tritter when the injected photons have polarisations as in Eqn. 8 of the main paper. In this case we inject photons into the first and second tritter inputs and monitor the first and second output ports. The solid line is the model curve, whilst the dashed line is an ideal theory curve. The model yields a visibility of 10%, while for the ideal curve the visibility is 12.5%. The FWHM of the model dip is ~ 150 fs. The slight gradient in the wings of the distribution is due to a change in coupling as a function of the translation stage position.

We also recorded coincidences for the outputs corresponding to $P_{210}, P_{201}, P_{300}$ but these statistics are all predicted to have lower visibilities for this case of $\varphi = \pi$ compared to $\varphi = 0$. Our recorded statistics are not sufficient to resolve these features.

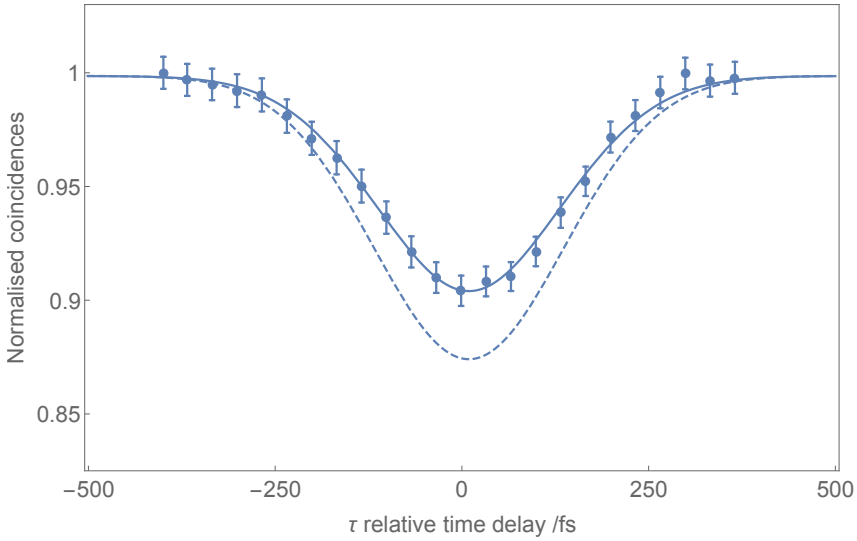

Figure 9. Plot of normalised heralded two-photon coincidences through the tritter when the injected photons have polarisations as in Eqn. 8 of the main paper. In this case we inject photons into the first and third tritter inputs and monitor the first and third output ports. The solid line is the model curve, whilst the dashed line is an ideal theory curve. The model yields a visibility of 10%, while for the ideal curve the visibility is 12.5%. The FWHM of the model dip is $\sim$ 300 fs.

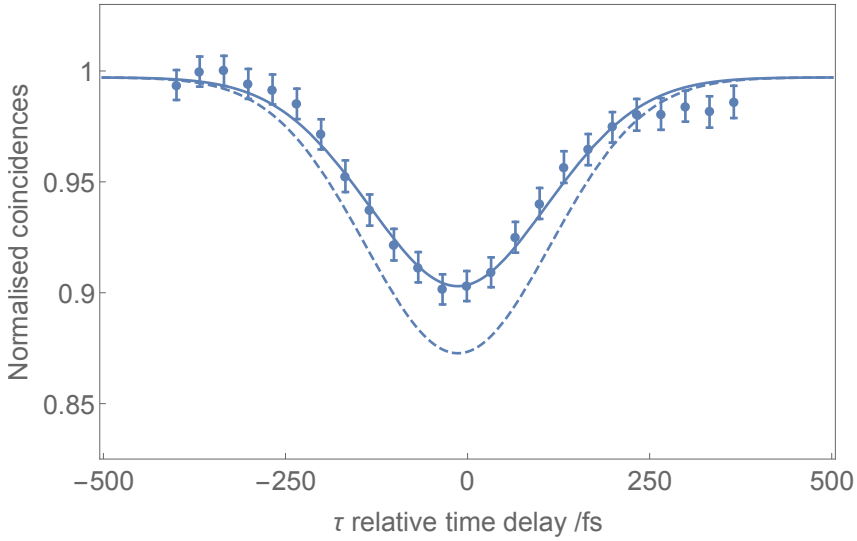

Figure 10. Plot of normalised heralded two-photon coincidences through the tritter when the injected photons have polarisation as in Eqn. 8 of the main paper. In this case we inject photons into the second and third tritter inputs and monitor the second and third output ports. The solid line is the model curve, whilst the dashed line is an ideal theory curve. The model yields a visibility of 10%, while for the ideal curve the visibility is 12.5%. The FWHM of the model dip is $\sim$ 300 fs. The slight difference in counts in the wings of the distribution is due to a change in coupling as a function of translation stage position.

Probing the triad phase (cf. Equation 9 in main paper)

Polarisation dependence of the tritter

For isolating three-photon interference, we scan the triad phase by varying the polarisation of one of the photons. In order to study the polarisation-dependence of the tritter, we send heralded single photons into different tritter inputs and record the output counts (see Figures 11 and 12).

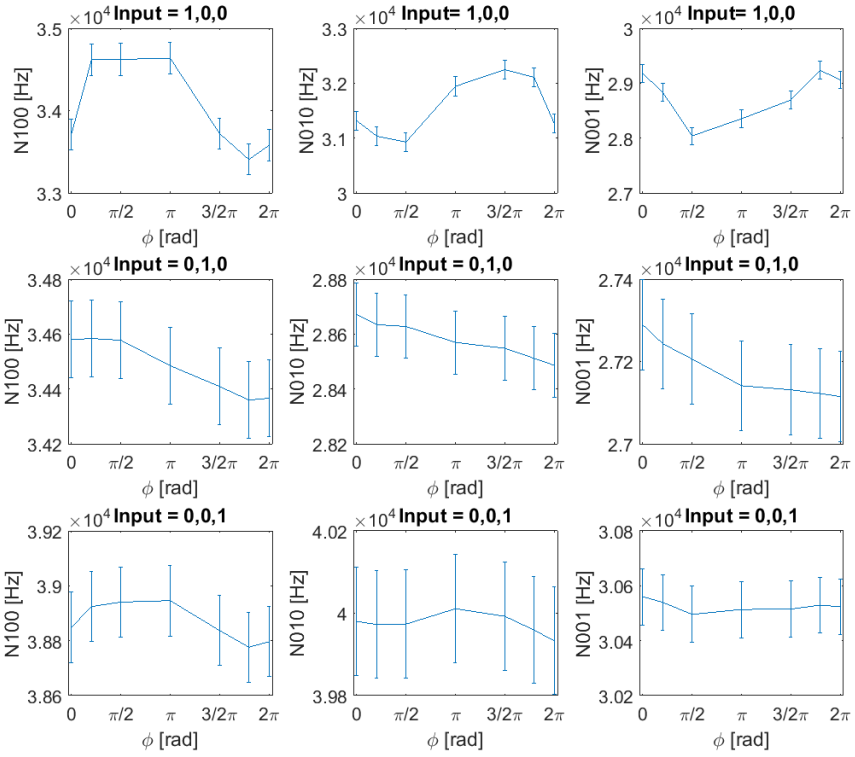

Figure 11. All input and output combinations for heralded single-photon events. The y-axis labels the count rates for a particular output configuration, and the x-axis is the triad phase we scan. The input port for the injected photon is labelled above each plot. The variation of the counts for the case where the polarisation of the photon is varied before injection (first row) shows that the tritter is slightly polarisation dependent: the coupling between spatial modes varies as a function of the triad phase. The slight drop of counts shown in the second row (where a single photon is injected into the second tritter input) is due to imperfect fibre coupling.

The total number of counts is relatively constant (see Fig. 12), whilst some individual heralded singles events in the top row of Figure 11 vary as the triad phase (and thus polarisation of the photon injected into the first input) changes. This suggests that the couplings of the tritter have a slight polarisation dependence.

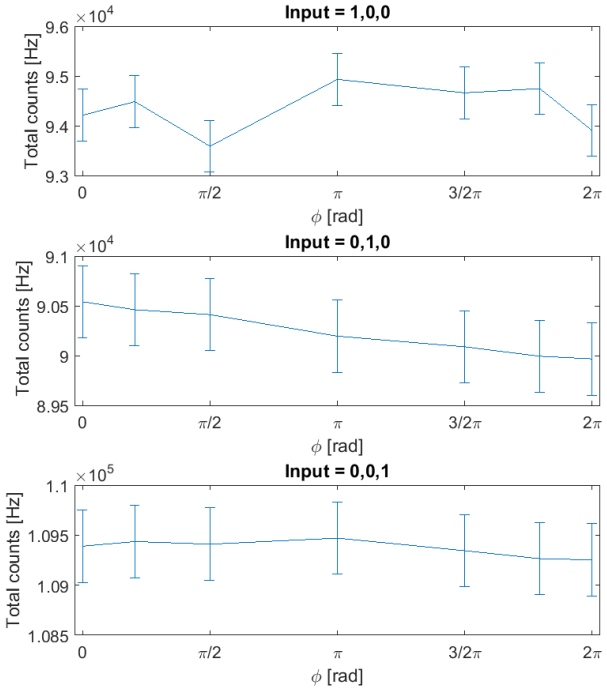

Figure 12. We plot the sum of all heralded single counts for different inputs into the tritter (total counts=N100+N010+N001, corresponding to summing the counts in the rows appearing in Figure 11).

Heralded two-photon coincidences

We monitored the heralded two-fold coincidences to verify that we have as little variation as possible as a function of the triad phase. In Figure 13 all possible combinations of heralded two-photon events are displayed. The largest variation in counts is observed for channels containing the first input channel, arising, as discussed in the previous section, from the tritter's polarisation dependence.

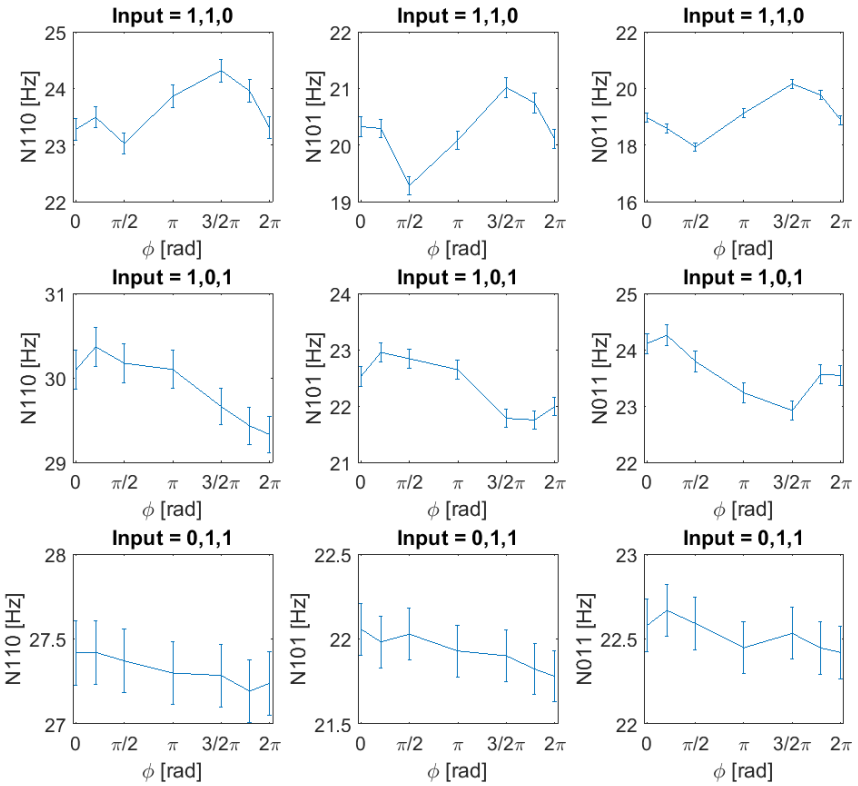

Figure 13. All input and output combinations for heralded two-photon events. We plot the number of heralded two-fold coincidences in the first and second (N110), first and third (N101), and second and third (N011) spatial output modes when changing the triad phase (and thus polarisation of the photon injected into the third input). The channels with the highest variation are those involving the first input channel, and this suggests it is due to the tritter's polarisation dependence.

Additional output event plots

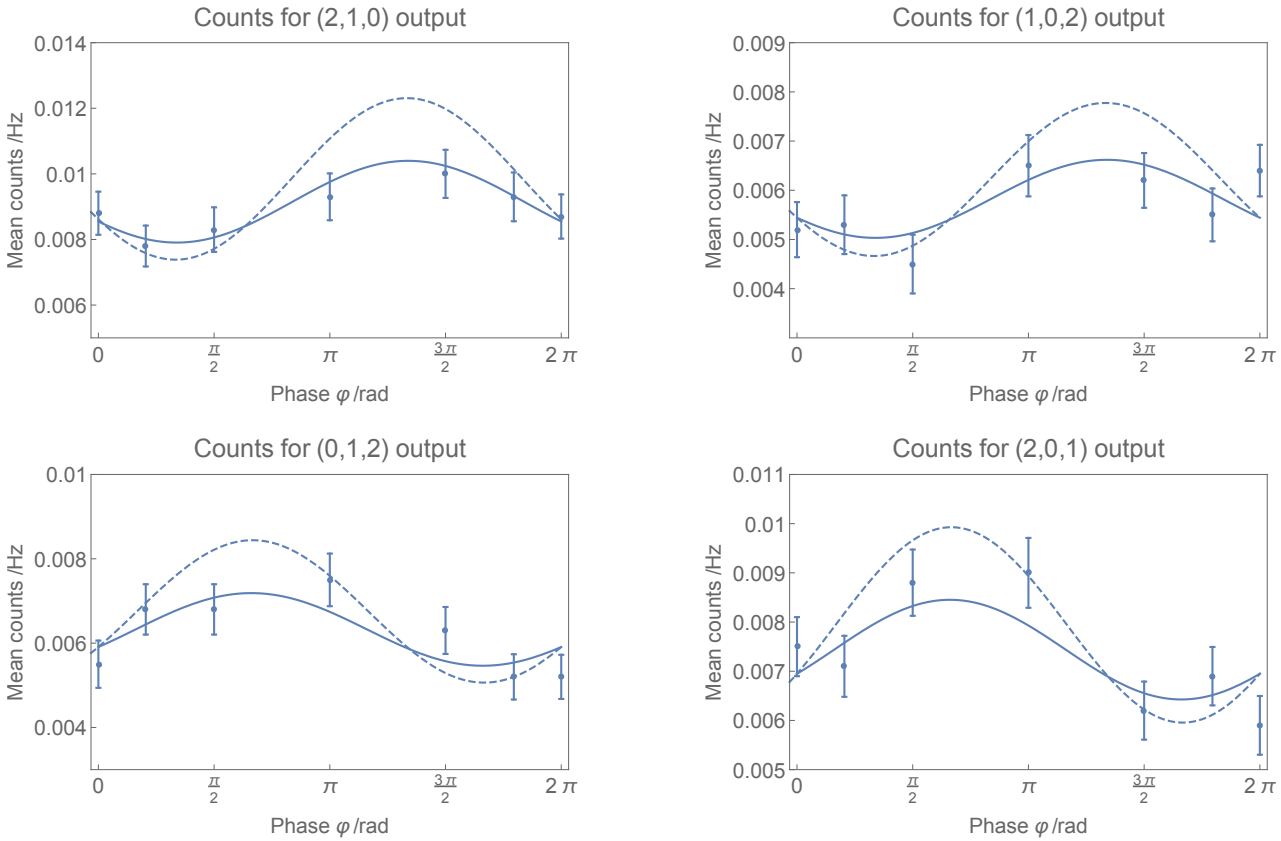

Figure 14. Plots for count rates corresponding to cases where two photons exit the same output port, whilst the third exits in a different port. From Eqns. 6 and 7 we expect cosine curves shifted by $-\pi/3$ for (2,1,0) and (1,0,2), and by $+\pi/3$ for (0,1,2) and (2,0,1). The solid lines are simulation curves and the dashed lines are ideal theory, and both have been normalised to fit the data at $\varphi = 0, 2\pi$ via a multiplicative scaling factor for comparison.

SIMULATION OF THE EXPERIMENT

Our experimental data show the expected behaviour, but there are some deviations from the probabilities given by theory. These are primarily due to an imperfect tritter operation, imperfections in the photon preparation (polarisation, purity ($P > 90\%$), distinguishability), and higher-order photon emission. Further, along with photons that are produced by the SFWM-process, uncorrelated photons are created in other processes such as Raman scattering and fluorescence [3]. To understand the influence of all these effects on the measured visibilities, we performed a simulation of our experiment. We used the formalism developed in [4–6] to simulate general mixed, squeezed states, contaminated with distinguishable noise photons, that are input into a lossy unitary. Our model includes terms corresponding to up to $N = 8$ photons in total (signals and heralds) and up to 3 uncorrelated noise photons. This provides sufficient accuracy as terms corresponding to higher photon numbers are negligibly small.

Impure input states

It was noted previously in [4] that the counting statistics for a mixed state input can be expressed as a function of the density matrices ρ_i for each photon in input mode i. For three photons input to an interferometer described by the unitary U this leads to the following expression for the coincidence probability P_{111}:

$$\begin{aligned} P_{111} = \mathrm{perm}(U * U^\star) + \mathrm{Tr}(\rho_1\rho_2)\mathrm{perm}(U * U^\star_{2,1,3}) + \mathrm{Tr}(\rho_1\rho_3)\mathrm{perm}(U * U^\star_{3,2,1}) + \mathrm{Tr}(\rho_2\rho_3)\mathrm{perm}(U * U^\star_{1,3,2}) \\ +2\mathrm{Re}(Tr(\rho_1\rho_2\rho_3))\mathrm{Re}(\mathrm{perm}(U * U^\star_{2,3,1})) - 2\mathrm{Im}(\mathrm{Tr}(\rho_1\rho_2\rho_3))\mathrm{Im}(\mathrm{perm}(U * U^\star_{2,3,1})) \end{aligned} \tag{30}$$

For simplicity in the simulation we make the assumption that we can decompose the density matrix into a mixed and a pure subspace, where the full density matrix for each photon is given by their tensor product:

$$\rho_i = \rho_{pure,i} \otimes \rho_{mixed,i} \tag{31}$$

ρ_{pure} may be represented as the tensor product of a density matrix which contains the temporal modes and another containing the polarisation degree of freedom.

$$\rho_{pure,i} = \rho_{temp,i} \otimes \rho_{pol,i} \tag{32}$$

For general temporal modes $|t_1\rangle, |t_2\rangle, |t_3\rangle$, we find a representation of the states in terms of orthonormal modes $|\tau_1\rangle, |\tau_2\rangle, |\tau_3\rangle$ using the Gram-Schmidt decomposition:

$$|t_1\rangle = |\tau_1\rangle \tag{33}$$

$$|t_2\rangle = \langle t_1|t_2\rangle|\tau_1\rangle + \sqrt{1 - |\langle t_1|t_2\rangle|^2}|\tau_2\rangle \tag{34}$$

$$|t_3\rangle = \langle t_1|t_3\rangle|\tau_1\rangle + \alpha|\tau_2\rangle + \sqrt{1 - |\alpha|^2 - |\langle t_1|t_3\rangle|^2}|\tau_3\rangle \tag{35}$$

Where $\alpha = \frac{\langle t_2|t_3\rangle - \langle t_2|t_1\rangle\langle t_1|t_3\rangle}{\sqrt{1-|\langle t_1|t_2\rangle|^2}}$
and $|t_1\rangle, |\tau_2\rangle, |\tau_3\rangle$ are a set of orthonormal vectors. We can then construct the density matrices in mode basis:

$$\rho_{temp,i} = |t_i\rangle\langle t_i| \tag{36}$$

The polarisation density matrix is constructed from basis states $|H\rangle$ and $|V\rangle$. Mixedness is modelled on a two dimensional Hilbert-space which is chosen to be orthogonal to time-frequency and polarisation modes.

Higher order photon contributions

The state of a single ideal two-mode-squeezer is given by:

$$|\Psi\rangle = \sqrt{1-\lambda^2}\sum_{n=0}^{\infty}\lambda^n|n_s n_i\rangle \tag{37}$$

Furthermore, we assume that in each source uncorrelated photons are created with probabilities P_I for the idlers and P_S for the signals. In particular $(1-P_I)(1-P_S)$ is the probability of producing no uncorrelated noise photons. $(1-P_I)P_I(1-P_S)P_S$ is the probability of creating exactly one uncorrelated photon pair.

We can then construct the density matrix for one source's emission:

$$\hat{\rho} = (1-\lambda^2)\cdot(1-P_I)\cdot(1-P_S)\sum_{n,k,l=0}^{\infty}\lambda^{2n}P_I^k P_S^l |n_s n_i, k_s l_i\rangle\langle n_s n_i, k_s l_i| \tag{38}$$

where for each total number of photons $2n+k+l$, we include cases where they come from four-wave mixing or noise processes. The indices k and l label the number of signal and idler noise photons which are assumed to be completely distinguishable from all other photons.

Parameter values

In the following table we give the parameter values that were used for the simulation:

Name	Symbol	Value
Squeezing-parameter	λ	0.16
Purity	$\mathcal{P}$	0.9
Fluorescence probability idler	P_I	0.035
Fluorescence probability signal	P_S	0.009

The squeezing parameter was taken to be the same as in [3]; the experiment reported in [3] was performed with the same power of the pump beam). The purity is a lower bound estimate and primarily affected by our ability to filter out non-factorable components in the (signal/idler) joint spectral distribution. We were limited in the signal/idler filtering bandwidth as we used a single pair of angle tuned bandpass filters in the beam path of signal and idler photons, immediately after a dichroic mirror. Since the three beams pass through the filters at slightly different angles the filters' spectral edges are slightly shifted with respect to each other, effectively limiting our tuning range. We calculate the degree of spectral purity for the given filter bandwidth of $10-15$ nm and obtain a value of approximately $\approx 90\%$ purity. The uncorrelated noise probability is obtained from a measurement of the heralded $g^{(2)}(0)$ in [3] (supplementary). We perform a fit of the $g^{(2)}(0)$ to our model and use P_I as a free parameter. P_S is chosen to be $1/4$ of P_I as the background noise for the signals is significantly smaller. The ratio of $\frac{P_S}{P_I} \approx 0.25$ was obtained by comparing background noise levels of signal and idler photons with a single photon spectrometer. When the pump polarisation is rotated by 90 degree we lose phase-matching, allowing us to observe the background noise only at the given input power.

[1] M. C. Tichy, Phys. Rev. A **91**, 022316 (2015).
[2] M. C. Tichy, M. Tiersch, F. de Melo, F. Mintert, and A. Buchleitner, Phys. Rev. Lett. **104**, 220405 (2010).
[3] J. B. Spring, P. L. Mennea, B. J. Metcalf, P. C. Humphreys, J. C. Gates, H. L. Rogers, C. Soeller, B. J. Smith, W. S. Kolthammer, P. G. Smith, *et al.*, arXiv preprint arXiv:1603.06984 (2016).
[4] M. C. Tichy, Y.-S. Ra, H.-T. Lim, C. Gneiting, Y.-H. Kim, and K. Mølmer, New J. Phys. **17**, 023008 (2015).
[5] V. S. Shchesnovich, Phys. Rev. A **91**, 063842 (2015).
[6] V. S. Shchesnovich, Phys. Rev. A **91**, 013844 (2015).